

LEARNING FLATNESS-BASED CONTROLLER USING NEURAL NETWORK

Hailin Ren

Robotics and Mechatronics Lab
Department of Mechanical Engineering
Virginia Tech,
Blacksburg, Virginia 24060

Jingyuan Qi

Department of Physics
Virginia Tech,
Blacksburg, Virginia 24060

Pinhas Ben-Tzvi *

Robotics and Mechatronics Lab
Department of Mechanical Engineering
Virginia Tech,
Blacksburg, Virginia 24060

ABSTRACT

This paper presents a method to imitate flatness-based controllers for mobile robots using neural networks. We present sample case studies for a unicycle mobile robot and an Unmanned Aerial Vehicle (UAV) quadcopter. The goals of this paper are to (1) train a neural network to approximate a previously designed flatness-based controller, which takes in the desired trajectories previously planned in the flatness space and robot states in a general state space, and (2) present a dynamic training approach to learn models with high dimension inputs. It is shown that a simple neural network could adequately compute the highly nonlinear state variables transformation from general state space to flatness space and replace the complicated designed heuristic to avoid the singularities in the control law. This paper also presents a new dynamic training method for models with high dimension independent inputs, serving as a reference for learning models with a multitude of inputs. Training procedures and simulations are presented to show both the effectiveness of this novel training approach and the performance of the well-trained neural network.

INTRODUCTION

Flat systems have gained popularity for analyzing and designing controllers for nonlinear systems due to their advantages in trajectory planning and tracking [1]. Flat outputs and their derivatives can be used to express the states and inputs of the original system or the extended system, simplifying the trajec-

tory planning problem to simple algebra [2] [3]. With the benefits of using a transformation based on the flatness property, a variety of interpolating functions can be used to design the path in the flat output space. This property attracts research in path planning and controllers design for various under-actuated systems, such as unicycles [4] [5], quadcopters [6] [7], open chain manipulators [8], etc.

In the last few decades, machine learning techniques have been used to solve a wide range of problems, such as human pose estimation [9], natural language processing [10], high-level motion/primitive tasks planning [11], and others. Using artificial neural networks to imitate system models and learn the suitable controllers is also an active topic in the research community. Inverse kinematics of a redundant manipulator are learned using neural networks in real time [12]. Three types of compensation methods were proposed to improve the inverse kinematics based controller for a robot manipulator [13]. Direct Online Optimization of Modeling Errors in Dynamics (DOOMED) is proposed to calculate the error between the real model and the analytic model to improve the control performance [14]. A closed-loop controller is then calculated to control a soft pneumatically actuated manipulator using Reinforcement Learning (RL) [15].

In this paper, we present methods to approximate flatness-based controllers using artificial neural networks including two popular case studies: a unicycle and a quadcopter. To deal with the high dimension inputs of the flatness-based controller model, we developed a dynamic sampling method to generate data batches for neural network training. Compared to using a static dataset, this dynamic sampling method uses and re-uses the same memory space periodically during the training process,

*Corresponding author – bentzvi@vt.edu

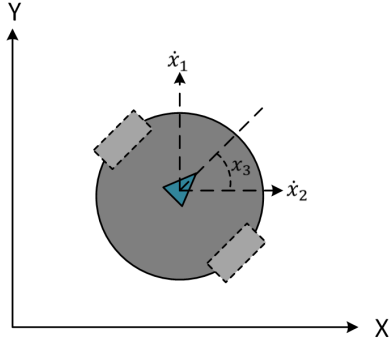


Figure 1. Kinematic model of a unicycle

thereby saving the overall memory space occupied. The authors believe this type of dataset generation will benefit research in learning models with large input dimension.

PRELIMINARY MODELING ANALYSIS

Kinematic Model of a Unicycle

Referring to a simple car model with two coaxial wheels as shown in Fig 1, two wheels are driven independently by two motors. The inputs to the system are the right and left wheel velocities, v_r and v_l , and the configuration of the system can be fully described by the general coordinates (x, y, ψ) , which encapsulates the chassis center position and heading angle. The system can be written in driftless affine-form as,

$$\dot{x} = \underbrace{\begin{pmatrix} \dot{x}_1 \\ \dot{x}_2 \\ \dot{x}_3 \end{pmatrix}}_{g_1(x)} = \begin{pmatrix} \sin(x_3) \\ \cos(x_3) \\ 0 \end{pmatrix} u_1 + \underbrace{\begin{pmatrix} 0 \\ 0 \\ 1 \end{pmatrix}}_{g_2(x)} u_2 \quad (1)$$

where x_1, x_2 stands for y and x positions, respectively, and x_3 for the heading. $u_1 = \frac{v_r + v_l}{2}$ is the rate of heading, $u_2 = \frac{v_r - v_l}{d}$ is the rate of rotation, and d is the wheel separation distance. It's easy to show that the local accessibility distribution of the car system, $\langle g_1(x), g_2(x), [g_1, g_2](x) \rangle$, is of full rank, where $[\cdot, \cdot]$ presents the Lie bracket operation. The local accessibility provides this driftless system with the necessary and sufficient conditions for controllability. It can be easily checked that the model of unicycle system Eq. 1 cannot be statically linearized. However, by extending the system based on a new state ($\bar{x}_4 = u_1$) while keeping others the same ($\bar{x}_i = x_i, i = 1, 2, 3$),

$$\begin{aligned} \dot{\bar{x}}_1 &= \sin(\bar{x}_3) \bar{x}_4 \\ \dot{\bar{x}}_2 &= \cos(\bar{x}_3) \bar{x}_4 \\ \dot{\bar{x}}_3 &= \bar{u}_2 \\ \dot{\bar{x}}_4 &= \bar{u}_1 \end{aligned} \quad (2)$$

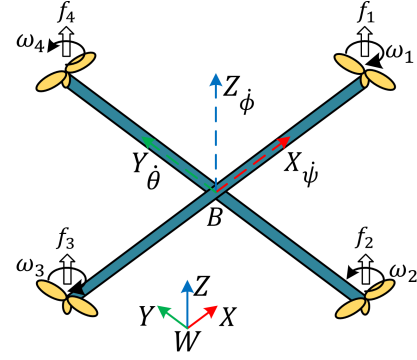


Figure 2. Dynamic model of a quadcopter

The extended system can be linearized to a new flat system with a transformation of variables, z ,

$$z = \begin{pmatrix} z_1 \\ z_2 \\ z_3 \\ z_4 \end{pmatrix} = \begin{pmatrix} \bar{x}_1 \\ \dot{\bar{x}}_1 \\ \bar{x}_2 \\ \dot{\bar{x}}_2 \end{pmatrix} = \begin{pmatrix} \bar{x}_1 \\ \bar{x}_4 \sin \bar{x}_3 \\ \bar{x}_2 \\ \bar{x}_4 \cos \bar{x}_3 \end{pmatrix} \quad (3)$$

The extended system can be written in Brunovsky form with a feedback law given as,

$$v = \begin{pmatrix} v_1 \\ v_2 \end{pmatrix} = \begin{pmatrix} \ddot{\bar{x}}_1 \\ \ddot{\bar{x}}_2 \end{pmatrix} = \begin{pmatrix} \sin(\bar{x}_3) & \bar{x}_4 \cos(\bar{x}_3) \\ \cos(\bar{x}_3) & -\bar{x}_4 \sin(\bar{x}_3) \end{pmatrix} \begin{pmatrix} \bar{u}_1 \\ \bar{u}_2 \end{pmatrix} \quad (4)$$

The system is now transformed via static feedback into a system which, in suitable coordinate, is fully linear and controllable. While adapting a classical polynomial control law for the new input variable v with disturbance compensation, the following equations can be obtained:

$$\begin{aligned} v_1 &= \ddot{\bar{x}}_1 + \lambda_1 \cdot e_{11} + \lambda_2 \cdot e_{21} + \lambda_3 \cdot e_{31} \\ v_2 &= \ddot{\bar{x}}_2 + \lambda_1 \cdot e_{12} + \lambda_2 \cdot e_{22} + \lambda_3 \cdot e_{32} \end{aligned} \quad (5)$$

where $e_{11} = \dot{\bar{x}}_1 - \dot{\bar{x}}_{1d}$, $e_{21} = \bar{x}_1 - \bar{x}_{1d}$, $e_{12} = \dot{\bar{x}}_2 - \dot{\bar{x}}_{2d}$, $e_{22} = \bar{x}_2 - \bar{x}_{2d}$, $e_{31} = \int \bar{x}_1 - \int \bar{x}_{1d}$ and $e_{32} = \int \bar{x}_2 - \int \bar{x}_{2d}$ stand for the error signals. \bar{x}_{1d} and $\dot{\bar{x}}_{1d}$ represent the desired output signals, corresponding to x_1, \dot{x}_1 . The coefficients $\lambda_i, i = 0, \dots, 5$ are to be specified in Tab. 2.

Dynamic Model of a Quadcopter

A quadcopter that is composed of four rotors is detailed in Fig. 2. Speeding up or slowing down either rotor couple can control Yaw angle ψ . Roll angle ϕ and Pitch angle θ allow the quadcopter to move in the Y and X directions, respectively. The rotor is the primary source of control and propulsion for the UAV. ZYX Euler angles (ψ, ϕ, θ) are applied with the conditions $(-\pi \leq \psi < \pi)$ for yaw, $(-\pi \leq \phi < \pi)$ for pitch, and $(-\pi \leq \theta < \pi)$ for roll.

The mapping between the the platform coordinate frame \mathbf{B} and the coordinate frame \mathbf{W} is achieved through a 3×3 rotation

matrix ${}^W\mathbf{R}_B$ involving the three Euler angles (ψ, θ, ϕ) . ${}^W\mathbf{R}_B$ is used for the Euler angle representation:

$${}^W\mathbf{R}_B = \begin{bmatrix} c\psi c\theta & c\psi s\phi s\theta - c\phi s\psi & s\phi s\psi + c\phi c\psi s\theta \\ c\theta s\psi & c\phi c\psi + s\phi s\psi s\theta & c\phi s\psi s\theta - c\psi s\phi \\ -s\theta & c\theta s\phi & c\phi c\theta \end{bmatrix} \quad (6)$$

where c and s denote cosine and sine, respectively. In the following, we use R to represent ${}^W\mathbf{R}_B$. Using Newtonian laws about the center of mass, the dynamic equations for the quadcopter are obtained:

$$m\dot{V}_0 = \sum F_{ext} \quad (7)$$

$$J\dot{\omega} = -\omega \times J\omega + \sum T_{ext} \quad (8)$$

where the symbol \times is the usual vector product, m is the mass, J is the inertia matrix which is given as a diagonal matrix:

$$J = \begin{pmatrix} I_x & 0 & 0 \\ 0 & I_y & 0 \\ 0 & 0 & I_z \end{pmatrix} \quad (9)$$

The coordinate frame is attached to the UAV body frame as shown in Fig. 2. The angular velocity $\omega = (\omega_x, \omega_y, \omega_z)^T$ and angular acceleration $\alpha = (\alpha_x, \alpha_y, \alpha_z)^T$ of the body frame with respect to frame \mathbf{B} are functions of the first and second time derivatives of the Euler angles $(\dot{\psi}, \dot{\theta}, \dot{\phi})$ and $(\ddot{\psi}, \ddot{\theta}, \ddot{\phi})$. Resolving the component of these derivatives along the axis of frame \mathbf{B} , we obtain,

$$\omega = \begin{pmatrix} \omega_x \\ \omega_y \\ \omega_z \end{pmatrix} = \begin{bmatrix} 1 & 0 & s\theta \\ 0 & c\psi & -s\psi c\theta \\ 0 & s\phi & c\phi c\theta \end{bmatrix} \begin{pmatrix} \dot{\psi} \\ \dot{\theta} \\ \dot{\phi} \end{pmatrix} \quad (10)$$

The angular acceleration of the UAV body frame with reference to frame \mathbf{B} is obtained:

$$\dot{\omega} = \begin{bmatrix} 1 & 0 & s\theta \\ 0 & c\psi & -s\psi c\theta \\ 0 & s\phi & c\phi c\theta \end{bmatrix} \begin{pmatrix} \ddot{\psi} \\ \ddot{\theta} \\ \ddot{\phi} \end{pmatrix} + \begin{bmatrix} 0 & 0 & \dot{\theta}c\theta \\ 0 & -\dot{\psi}s\psi & -\dot{\psi}c\psi c\theta + \dot{\theta}s\psi s\theta \\ 0 & \dot{\psi}c\psi & -\dot{\psi}s\psi c\theta - \dot{\theta}c\psi s\theta \end{bmatrix} \begin{pmatrix} \dot{\psi} \\ \dot{\theta} \\ \dot{\phi} \end{pmatrix} \quad (11)$$

The notations $\sum F_{ext}, \sum T_{ext}$ stand for the vector of external forces and torques, respectively. They can be computed as,

$$\sum F_{ext} = \begin{pmatrix} A_x - (s\psi s\phi + c\psi c\phi s\theta)u_1 \\ A_y - (s\psi c\phi s\theta - c\psi s\phi)u_1 \\ A_z + mg - c\phi c\theta u_1 \end{pmatrix} \quad (12)$$

$$\sum T_{ext} = \begin{pmatrix} A_p + u_2 d \\ A_q + u_3 d \\ A_r + u_4 \end{pmatrix} \quad (13)$$

where (A_x, A_y, A_z) and (A_p, A_q, A_r) are aerodynamic forces and moments acting on the UAV. u_1 is the resulting thrust of the four rotors defined as $u_1 = (F_1 + F_2 + \dots + F_4)$; u_2 is the difference of thrust between the left rotor and the right rotor defined as $u_2 = F_4 - F_2$; u_3 is the difference of thrust between the back rotor and the front rotor, defined as $u_3 = F_3 - F_1$; u_4

is the difference of torque between the two clockwise-turning rotors and the two counterclockwise-turning rotors, defined as $u_4 = C_{fm}[(F_1 + F_3) - (F_2 + F_4)]$, and C_{fm} is the force to moment scaling factor.

To avoid Lie transformation matrices singularity, we replace the real control signals (u_1, u_2, u_3, u_4) with $(\bar{u}_1, \bar{u}_2, \bar{u}_3, \bar{u}_4)$. u_1 is delayed by a double integrator, while the other control signals are unaltered by the variable transformation.

$$u_1 = \zeta; \dot{\zeta} = \xi; \dot{\xi} = \bar{u}_1; u_2 = \bar{u}_2; u_3 = \bar{u}_3; u_4 = \bar{u}_4 \quad (14)$$

The resulting system then can be described by state space equations in the following form:

$$\dot{x} = \bar{f}(x) + \sum_{i=1}^4 \bar{g}_i(x)\bar{u}_i \quad (15)$$

$$y = h(x)$$

where $x = (x, y, z, \psi, \phi, \theta, \dot{x}, \dot{y}, \dot{z}, \zeta, \xi, p, q, r)$, $y = (x, y, z, \psi)$, and,

$$f = \begin{pmatrix} \dot{x} \\ \dot{y} \\ \dot{z} \\ qs\phi s_e\theta + rc\phi s_e\theta \\ qc\phi - rs\phi \\ p + qs\phi t\theta + rc\phi t\theta \\ \frac{A_x}{m} - \frac{1}{m}(s\phi s\psi + c\phi c\psi s\theta)\zeta \\ \frac{A_y}{m} - \frac{1}{m}(c\phi s\psi s\theta - s\phi c\psi s\theta)\zeta \\ \frac{A_z}{m} + g - \frac{1}{m}(c\phi c\theta)\zeta \\ \xi \\ 0 \\ \frac{I_y - I_z}{I_x}qr + \frac{A_p}{I_x} \\ \frac{I_z - I_x}{I_y}pr + \frac{A_q}{I_y} \\ \frac{I_x - I_y}{I_z}pq + \frac{A_r}{I_z} \end{pmatrix} \quad (16)$$

$$\bar{g}_1 = \frac{\partial}{\partial x_{11}}, \bar{g}_2 = \frac{d}{I_x} \frac{\partial}{\partial x_{12}}, \bar{g}_3 = \frac{d}{I_y} \frac{\partial}{\partial x_{13}}, \bar{g}_4 = \frac{1}{I_z} \frac{\partial}{\partial x_{14}}$$

The input-output decoupling problem is solvable for the nonlinear system by means of static feedback, and the vector relative degree r_1, r_2, r_3, r_4 is given by $r_1 = r_2 = r_3 = 4; r_4 = 2$. We choose the flatness outputs as,

$$y = [y_1, y_2, y_3, y_4]^T = [x, y, z, \psi]^T \quad (17)$$

then obtain a feedback control law,

$$v = [y_1^{r_1}, y_2^{r_2}, y_3^{r_3}, y_4^{r_4}]^T = b(x) + \Delta(x)\bar{u} \quad (18)$$

where v represents the new input control signals. The matrix $\Delta(x)$ is non singular everywhere in the region $\zeta \neq 0, -\frac{\pi}{2} < \theta < \frac{\pi}{2}, -\frac{\pi}{2} < \phi < \frac{\pi}{2}$. Therefore, the input-output decoupling problem is solvable for our system by means of a control law in the form of:

$$\bar{u} = \alpha(x) + \beta(x)v \quad (19)$$

Table 1. Mass-properties of the quadcopter

Parameter	Description	Value	Units
Gravity	g	9.81	[m/s ²]
Quadcopter diameter	d	0.45	[m]
Mass	m	0.468	[Kg]
Quadcopter inertia	$I_{x,y,z}$	$4.9 \cdot 10^{-3}$	[Kg·m ²]

where,

$$\alpha(x) = -\Delta^{-1}(x)b(x) \quad (20)$$

$$\beta(x) = \Delta^{-1}(x) \quad (21)$$

The system can be transformed via static feedback into a system which, in suitable coordinates, is fully linear and controllable. While adapting a classical polynomial control law for the new input variable v with disturbance compensation, the following set of equations can be obtained:

$$\begin{aligned} v_1 &= x_d^{(4)} - \lambda_3 \ddot{e}_{11} - \lambda_2 \dot{e}_{11} - \lambda_1 e_{11} - \lambda_0 e_{11} \\ v_2 &= y_d^{(4)} - \lambda_3 \ddot{e}_{12} - \lambda_2 \dot{e}_{12} - \lambda_1 e_{12} - \lambda_0 e_{12} \\ v_3 &= z_d^{(4)} - \lambda_3 \ddot{e}_{13} - \lambda_2 \dot{e}_{13} - \lambda_1 e_{13} - \lambda_0 e_{13} \\ v_4 &= \ddot{\psi}_d - \lambda_5 \dot{e}_5 - \lambda_4 e_5 \end{aligned} \quad (22)$$

where x_d, y_d, z_d, ψ_d represent the desired output signals, corresponding to x, y, z, ψ , respectively, and the error signals $e_{11} = x_0 - x_{0d}, e_{12} = y_0 - y_{0d}, e_{13} = z_0 - z_{0d}$, and $e_5 = \psi - \psi_d$. The coefficients $\lambda_i, i = 0, \dots, 5$ are specified in Tab. 2.

The mass-properties of the quadcopter in our case study are chosen as shown in Tab. 1. Table 2 overviews the controller parameters used in the unicycle controller and the quadcopter controller. In the quadcopter control, only the body positions x, y, z are of interest, and the control parameters of the yaw control are set to zeros, $\lambda_4 = \lambda_5 = 0$.

DESIGNING FLATNESS-BASED CONTROLLER

Dynamic Sampling Approach

Generalization over the entire input space is one of the principles to estimate the performance of the trained neural network in machine learning. One way to achieve generalization is to create a large enough dataset that covers the entire input space, while the other is to split the dataset into a training set and a validation set. The former ensures generalization, but is computationally expensive, especially when applied in problems with

Table 2. Controller parameters for the unicycle and quadcopter

	λ_0	λ_1	λ_2	λ_3
unicycle	N/A	0.085	0.0025	0.0001
quadcopter	0.0025	0.0025	1.0000	0.0100

high input dimension, and is often infeasible in continuous input problems [16]. The latter helps avoid over-training in the subset, but is prone to fail when the dataset is not large enough or only partially covers the input space [17].

To deal with the proposed high dimension continuous input problems, we propose a dynamic sampling approach that marginally splits the entire workspace into a training set and a validation set. For a problem with n dimension inputs, $x = [x_1, x_2, \dots, x_n]$, with their lower boundaries, x_i^l , and upper boundaries, x_i^u . Discretization is applied to each input x_i uniformly into n_i bins with a fixed interval δ_i for x_i . The dataset is now converted to a finite set, $X_{data} = \{[x_1, x_2, \dots, x_n], x_i \in \{x_i^l, x_i^l + \delta_i, x_i^l + 2\delta_i, \dots, x_i^u\}\}$. The size of the dataset X_{data} increases dramatically when the input dimension increases and when the discretization becomes denser. Instead of storing the whole dataset, only the relatively smaller set, the validation dataset X_{valid} , is stored during the training process. To recover the continuous input space, sampling is performed based on the discrete data using a predefined distribution. The training procedure with dynamic sampling approach is described in the form of following pseudocode:

procedure Training Network

($\{x_i^l\}, \{x_i^u\}, n_i$)

- 1: Obtain discretization interval δ_i for x_i
- 2: Randomly generate validation set X_{valid}
- 3: **for** each training epoch, **i do**
- 4: **for** each training batch, **j do**
- 5: Generate discrete training set $x_{batch}^d \in \{x | x \in X_{data} - X_{valid}\}$ based on $\{x_i^l\}, \{x_i^u\}$
- 6: Generate continuous training set x_{batch}^c on the distribution over x_{batch}^d
- 7: Training neural network using x_{batch}^c
- 8: **end for**
- 9: **end for**

Here we applied i.i.d Gaussian sampling to the selected discrete training set to recover to continuous space, $x_{batch}^c \sim p(x_{batch}^d | \{\delta_i\})$. For data along each dimension, the selected discrete value is used as the mean value, $\mu = x^d$, while the standard deviation is selected to be the discretization interval $\sigma = \delta$. The generated training data along each dimension obeys Gaussian distribution, $x^c \sim \mathcal{N}(x^d, \delta)$. To avoid overfitting on any specific trajectory, the boundaries of the inputs, $\{x_i^l, x_i^u\}$, were provided by generating random trajectories using patterns such as a circle, a square, and a line. These inputs domains were then discretized and divided into training and validation datasets.

Neural Network Design and Training

Neural networks are widely used to better approximate highly nonlinear models or models with uncertainty to increase

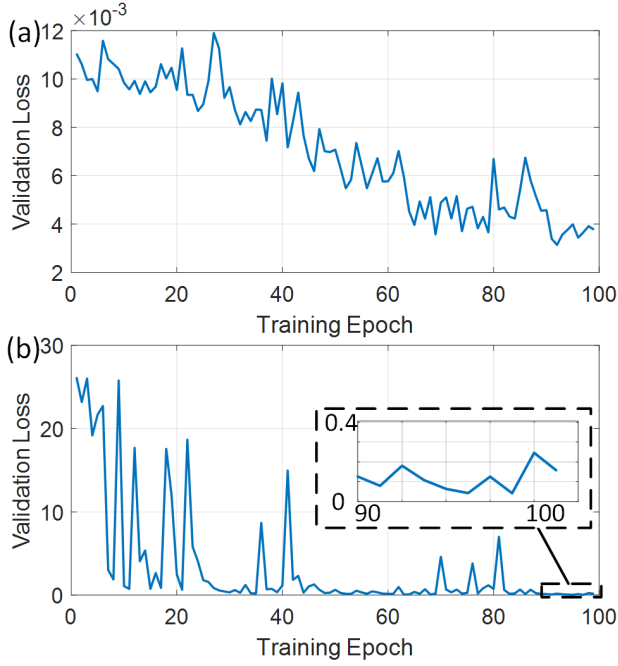


Figure 3. Training process of (a) the kinematic model of the unicycle, and (b) the dynamic model of the quadcopter

the performance and stability of controllers. To approximate the flatness-based controller of the unicycle and the quadcopter, Multilayer Perceptron (MLP) neural network is used. The proposed neural network consists of the fully connected neurons in each layer with linear activation function in all neurons. The neural network is built using Keras [18] with TensorFlow [19] as the backend. Hyperopt [20] is used to tune the hyperparameters of the neural network including number of layers n_l , number of neurons in each layer n_n , activation functions used for neurons in each layer except the final output layer f_a , and the parameters for the activation if needed f_p . Details of the choices and selected choices of the hyperparameters are presented in Tab. 3. The proposed neural network consists of 5 layers with 512 neurons in each layer. An activation function in each neuron is selected to be Leaky ReLU [21] with $\alpha = 0.5$ for the optimal performance.

Based on control laws in Eq. (4) and Eq. (5) for the unicycle, and Eq. (19) and Eq. (22) for the quadcopter, the neural network

Table 3. Hyperparameters tuning for neural network

Parameters	Choices	Selected
n_l	[4, 5, 6, 7, 8]	5
n_n	[128, 256, 512, 1024]	512
f_a	['ReLU', 'Sigmoid', 'Leaky ReLU']	'Leaky ReLU'
f_p	[0.1, 0.3, 0.4, 0.5, 0.7, 0.9]	0.5

Table 4. Loss weights used for the optimization

ω_i	\bar{u}_1	\bar{u}_2	\bar{u}_3	\bar{u}_4
unicycle	1	1	N/A	N/A
quadcopter	1000	1000000	100000	100000000

takes in the error signals and states and outputs the control signals for the model. We define our objective function to minimize the weighted loss function based on the order of magnitude of our controller outputs:

$$\min_{\Theta} L = \sum_{i=1}^n \omega_i \|\bar{u}_i - \bar{u}_i^{\Theta}\|_2 \quad (23)$$

where Θ represents the trainable parameters of the neural network, ω_i is the weight for the loss of the i -th outputs, \bar{u}_i is the output value from the flatness-based controller and is used as the ground truth, while \bar{u}_i^{Θ} is the estimated output from the neural network. For the unicycle controller, $n = 2$ outputs are designed in the neural network with the loss weights $\omega_1 = \omega_2 = 1$, while the neural network of the quadcopter controller generates $n = 4$ outputs with loss weights, as shown in Tab. 4. The training process includes 100 training epochs. Within each training epoch, 1000 training batches are performed, followed by validation using 100 batches of data. Weighted Root Mean Square Error (WRMSE) is used in the validation process:

$$WRMSE = \sqrt{\frac{\sum_{i=1}^n \omega_i (\bar{u}_i - \bar{u}_i^{\Theta})^2}{n}} \quad (24)$$

Figure 3 shows the training processes of flatness-based controllers for the unicycle and the quadcopter. It can be seen that the validation loss decreases as the training process progresses. It can be seen that the validation error, WRMSE, converges to approximately 4×10^{-3} for the unicycle model and approximately 0.1 for the quadcopter model.

VALIDATION OF PROPOSED APPROACH

To evaluate the performance of the well-trained controller using neural network in real applications, we compared our trained controller to the mathematical model-based controller in three different motions. For the unicycle, point-to-point, square, and circle motions are performed. The quadcopter performs similar motions in 3D with various vertical heights. The simulation was performed using Simulink [22] as shown in Fig. 4. All trajectories are generated using the trajectory planner. The desired trajectories are then sent to the controller, which could be either the well-trained neural network controller or the flatness-based controller that uses an explicit mathematical model. The simulated model uses controller outputs for its calculations.

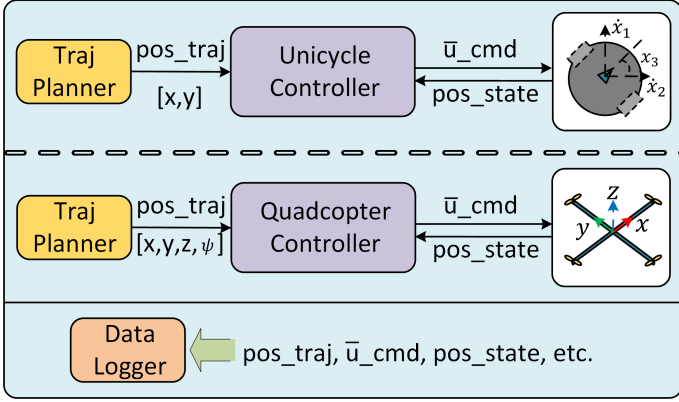


Figure 4. Simulation system for the unicycle and the quadcopter

Trajectory Planner

Given the diffeomorphism in Eq. (3) and Eq. (17), a point-to-point motion planning and tracking control can be designed in a flatness workspace. For example in the unicycle problem, given the terminal conditions in the Cartesian coordinates at both start time t_0 and final time t_f , $\{x_i(t), \dot{x}_i(t); i \in \{1, 2, 3\}, t \in \{t_0, t_f\}\}$, the terminal conditions can be transformed to the corresponding terminal conditions in the flatness workspace, $\{\bar{x}_i(t), \dot{\bar{x}}_i(t), \ddot{\bar{x}}_i(t); i \in \{1, 2\}, t \in \{t_0, t_f\}\}$. To satisfy these six terminal conditions, we choose three types of functions as trajectories for $\bar{x}_i(t); i \in \{1, 2\}$: fifth-order polynomials, trigonometric functions, and piecewise functions. For fifth-order polynomials, we used the following functions:

$$\bar{x}_i(t) = a_5 t^5 + a_4 t^4 + a_3 t^3 + a_2 t^2 + a_1 t + a_0 \quad i = \{1, 2\} \quad (25)$$

For trigonometric functions, we choose following functions:

$$\begin{aligned} \bar{x}_1(t) &= r \cdot \cos(2\pi \cdot t/T) \\ \bar{x}_2(t) &= r \cdot \sin(2\pi \cdot t/T) \end{aligned} \quad (26)$$

where r is the radius of the circle and T is the period in which the unicycle runs around the circle. The desired trajectory is a circle that starts from (10,0) at the top, running clockwise with radius 10 meters, all the way back to (10,0). In the simulation, we choose the real initial point to be (-0.5,8) to test the convergence.

We choose the following formula for our piecewise function:

$$\bar{x}_i(t) = \begin{cases} a_{51}t^5 + a_{41}t^4 + a_{31}t^3 + a_{21}t^2 + a_{11}t + a_{01} & 0 < t \leq t_1 \\ a_{52}t^5 + a_{42}t^4 + a_{32}t^3 + a_{22}t^2 + a_{12}t + a_{02} & t_1 < t \leq t_2 \\ a_{53}t^5 + a_{43}t^4 + a_{33}t^3 + a_{23}t^2 + a_{13}t + a_{03} & t_2 < t \leq t_3 \\ a_{54}t^5 + a_{44}t^4 + a_{34}t^3 + a_{24}t^2 + a_{14}t + a_{04} & t_3 < t \leq t_4 \end{cases} \quad i = \{1, 2\} \quad (27)$$

The desired trajectory, $(\bar{x}_1(t), \bar{x}_2(t))$, is a square, going from (0,0) to (0,24), then to (24,24), then (24,0), and finally back to (0,0). In the simulation, we choose the real initial point at (-2,2) to test convergence.

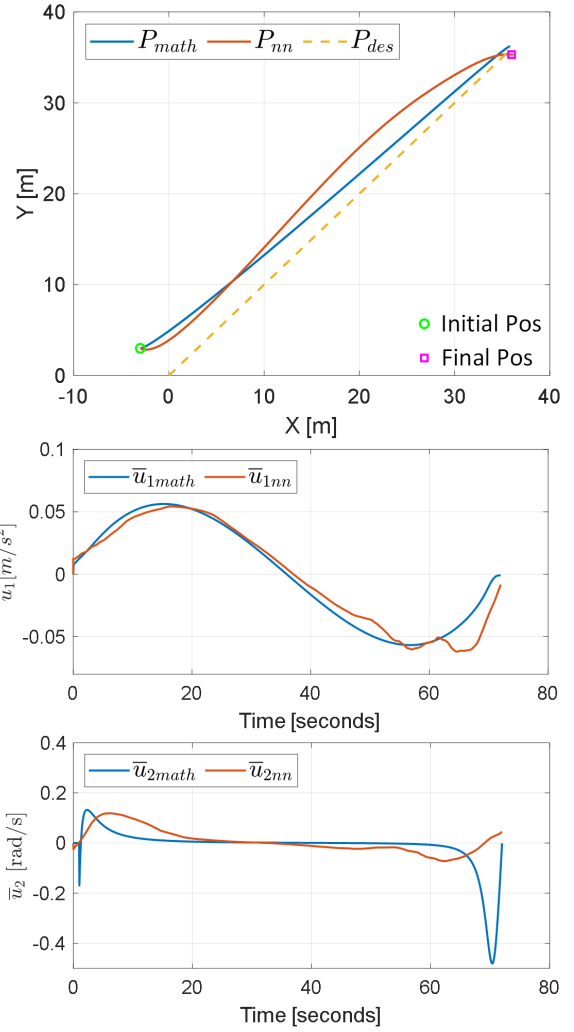


Figure 5. Point-to-point motion for the unicycle

A similar approach was used in the quadcopter process. We choose the same three types of trajectory functions that were used in the unicycle model. For the fifth order polynomials, we choose the same function as Eq. (25). For trigonometric functions of the quadcopter, we appended one more function to Eq. 26 to accommodate for the motion in the Z direction:

$$\bar{x}_3(t) = -1 - t/10 \quad (28)$$

where \bar{x}_3 is the position along the Z direction, representing height. The desired trajectory, $(\bar{x}_1(t), \bar{x}_2(t), \bar{x}_3(t))$, represents a circle, that starts from (0,15,-1) at the top, running clockwise with radius 10 meters all the way to (0,15,-1-10/t). The quadcopter simultaneously decreases its height at a constant rate. In the simulation, we choose the real initial point at (1,2,3) to test convergence. Eq. (27) is used as our piecewise function. The desired trajectory takes the form of a square going from (0,0,0)

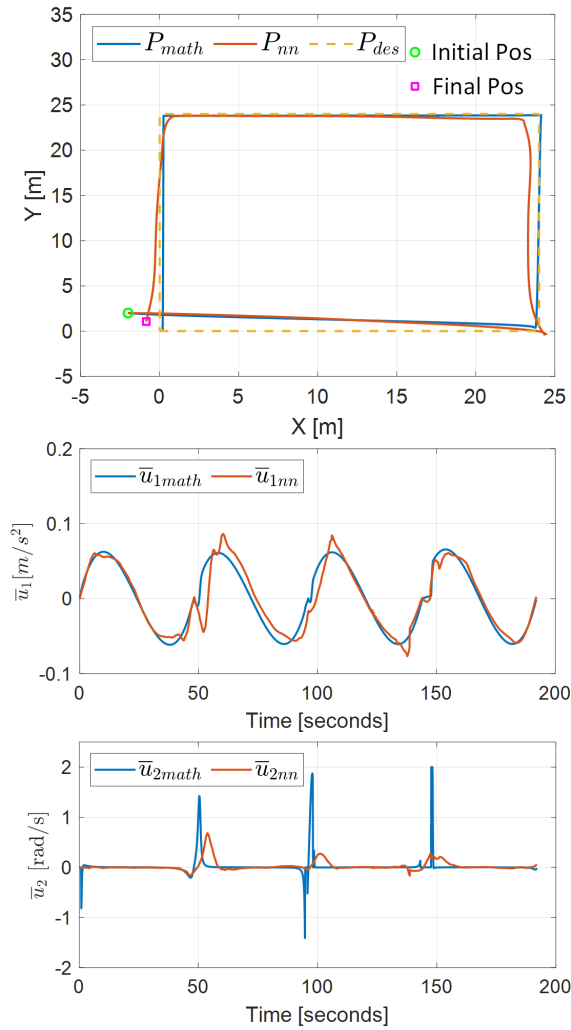


Figure 6. Square motion for the unicycle

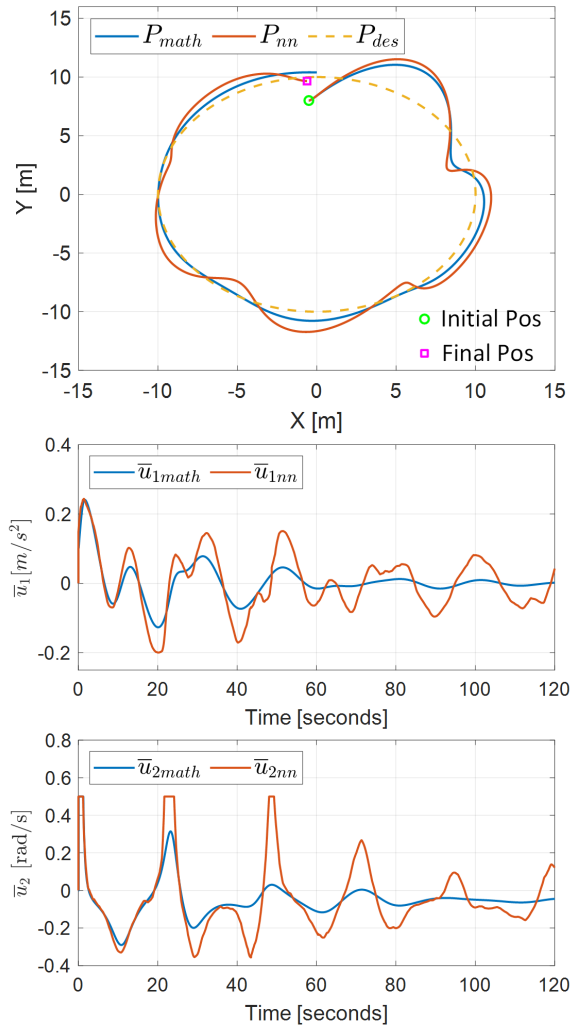


Figure 7. Circle motion for the unicycle

to (45,0,55), then to (45,45,0), then (0,45,55), and finally back to (0,0,0). In the simulation, we choose the real initial point to be (1,2,3) to test the convergence.

Trajectory Tracking Performance

Three motions of the unicycle were performed and compared in Figs. (5~7) while these of the quadcopter are presented in Figs. (8~10). One of the most straightforward measures of controller performance is evaluating the average deviation from the desired trajectory over the whole tracking process, using Root Mean Square Error (RMSE) and setting all weights to 1 in Eq. (24),

$$RMSE = \sqrt{\frac{1}{n} \sum_{i=1}^n \|f_i - g_i\|_2^2} \quad (29)$$

where f_i and g_i are the two compared trajectories at timestep i . Another way to measure controller performance is to capture the maximum "overshoot" during the tracking process, using the maximum absolute deviation values,

$$MAD = \max \|f_i - g_i\|_2 \quad (30)$$

where f_i and g_i are the two compared trajectories at timestep i . Similarly, these criteria can be used to estimate the imitation performance of the neural network controller to the explicit mathematical model based controller. Table 5 shows the performance criteria based on the three motions. It can be seen that the neural network-based controller obtained similar performance as the mathematical model-based controller. Compared to the mathematical model-based controller, the neural network-based controller applied larger control inputs in the unicycle problem. This could have been due to the limited size of the neural network or

Table 5. Performance on different motions

Unicycle				
	math ¹		nn ²	
	RMSE	MAD	RMSE	MAD
linear	2.407	2.007	3.035	2.801
square	1.014	0.689	1.970	1.665
circle	0.899	0.700	1.346	1.208
Quadcopter				
	math		nn	
	RMSE	MAD	RMSE	MAD
linear	1.834	1.345	1.836	1.356
square	1.320	2.393	1.803	3.255
circle	4.825	9.448	4.754	9.290

¹ math: mathematical model-based controller

² nn: neural network-based controller

the uniqueness of the path.

CONCLUSION AND FUTURE WORK

In this work, we accurately approximated flatness-based controllers using neural networks. We presented two case studies, a kinematic model for a unicycle and a dynamic model for a quadcopter. A dynamic sampling method was proposed to avoid large memory allocation during the training for problems with high input dimension. We simulated a well-trained model using three different motions and quantified the imitating performance of our neural network controller in comparison to a mathematical model-based controller. It was shown that the neural network-based controller was able to emulate two complex non-linear controllers. The proposed method of dynamic sampling is also useful for training high-input-dimension neural networks with ground truth modeling, which is not limited to the presented study cases. The well trained controller can be further integrated with high level controllers or task planners that are neural network based or heuristic.

Future work involves training the neural network controller using real world data to include the uncertainty in mathematical modeling to make it more robust and stable. Sampling methods and neural network architectures need to be improved to perform adequate learning with limited real world data, as real world data collection is expensive in comparison to generating data from a simplified simulated model. Also, a transfer learning framework or conditional neural network could be developed to handle the cases where model parameters change.

ACKNOWLEDGMENT

The authors would like to gratefully acknowledge the support of NVIDIA Corporation with the donation of the Titan Xp GPU used for this research.

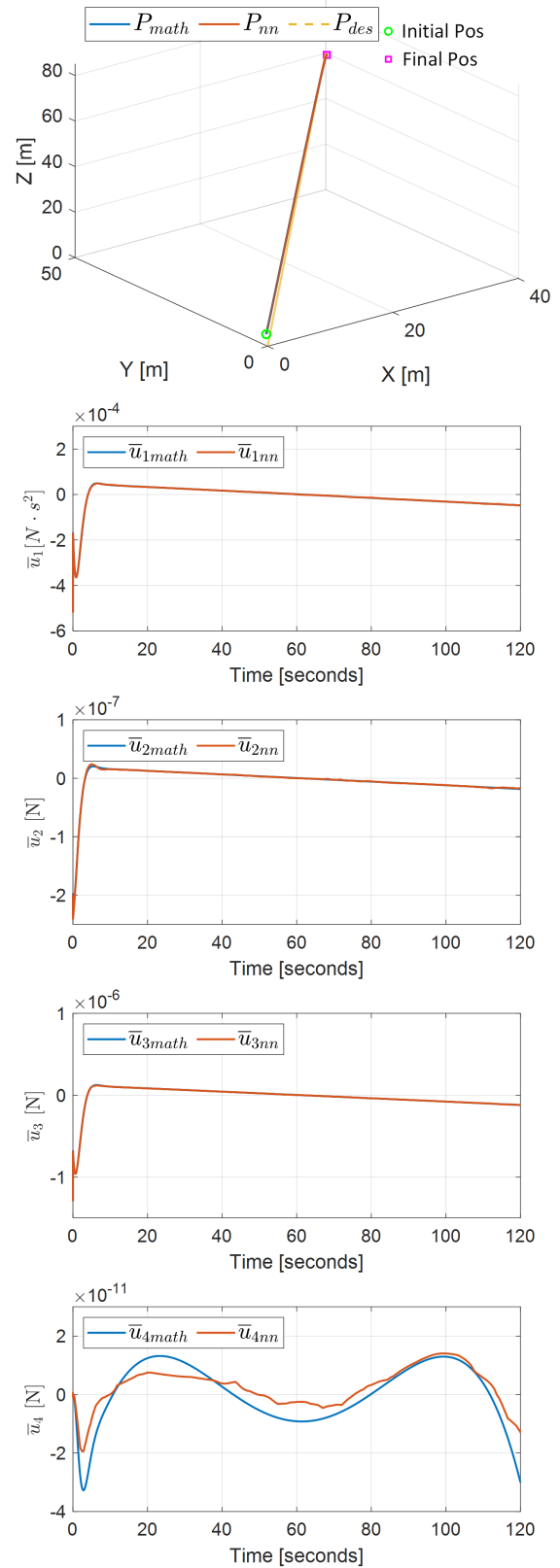


Figure 8. Point-to-point motion for the quadcopter

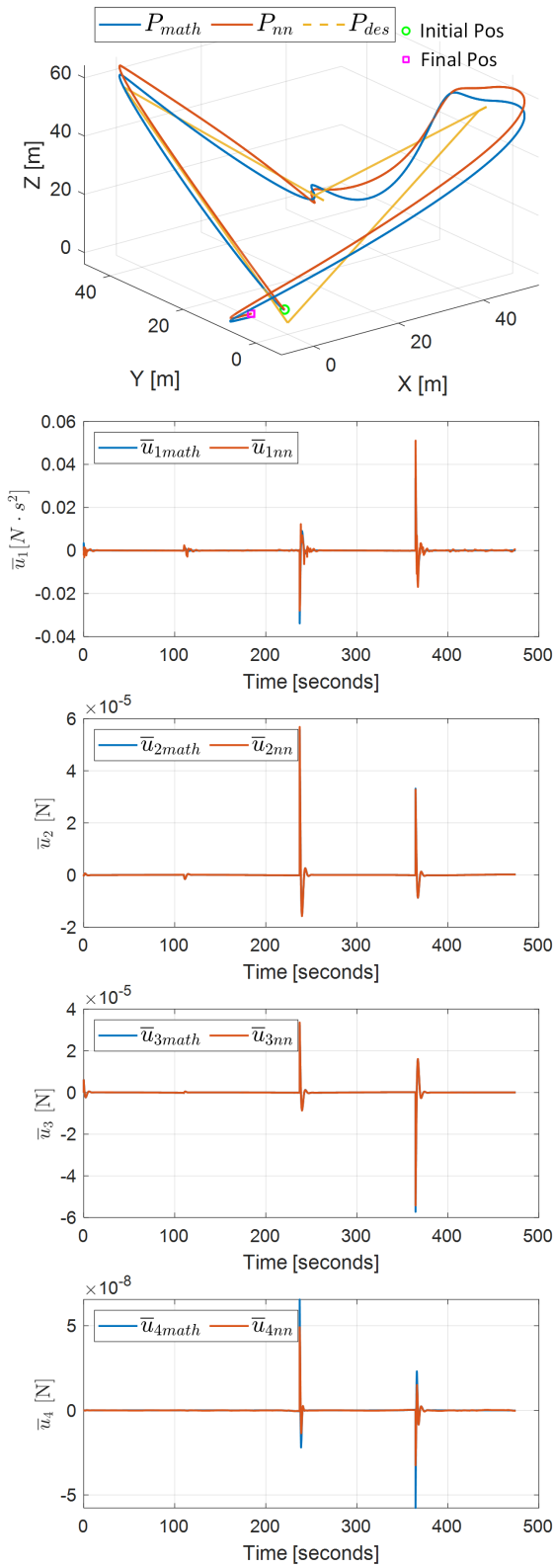


Figure 9. Square motion for the quadcopter

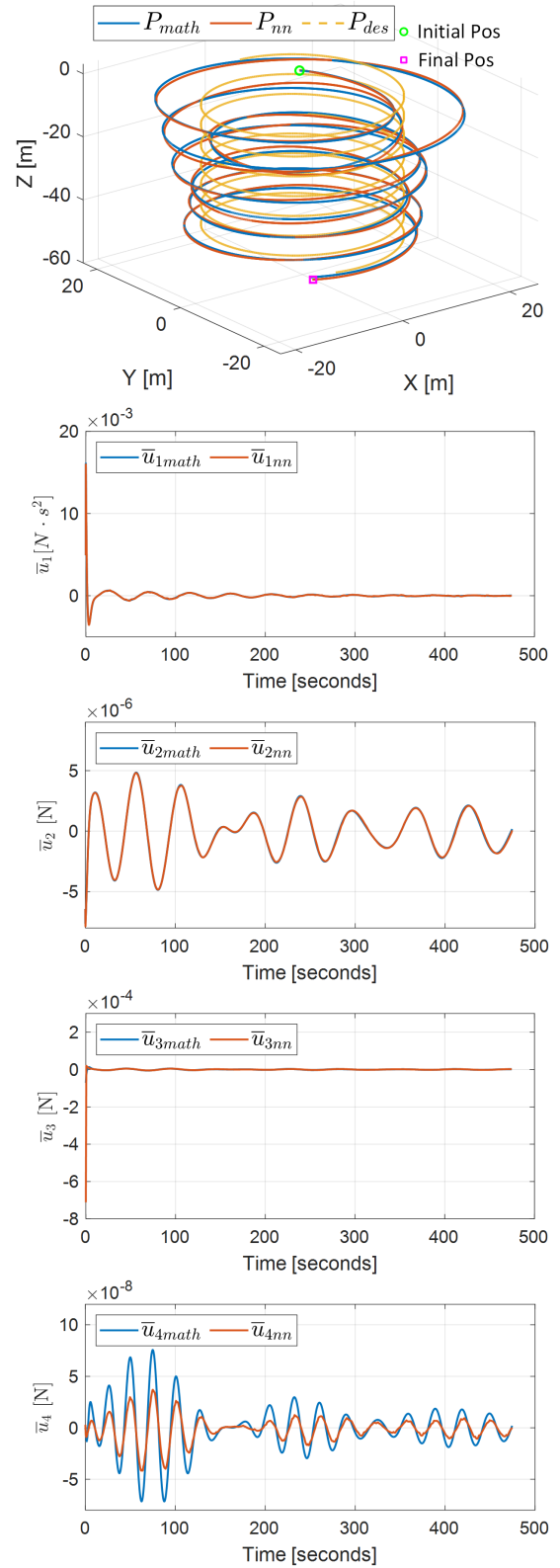


Figure 10. Circle motion for the quadcopter

REFERENCES

- [1] Sira-Ramírez, H., and Agrawal, S., 2004. *Differentially Flat Systems*. CRC Press, 5.
- [2] Francisco, S., Murray, R. M., Rathinam, M., and Sluis, W., 1995. “Differential Flatness of Mechanical Control Systems: A Catalog of Prototype Systems”. In Proceedings of the 1995 ASME International Congress and Exposition.
- [3] Soheil-Hamedani, M., Zandi, M., Gavagsaz-Ghoachani, R., Nahid-Mobarakeh, B., and Pierfederici, S., 2016. “Flatness-based control method: A review of its applications to power systems”. In 2016 7th Power Electronics and Drive Systems Technologies Conference (PEDSTC), IEEE, pp. 547–552.
- [4] Tang, C. P., 2009. “Differential flatness-based kinematic and dynamic control of a differentially driven wheeled mobile robot”. In 2009 IEEE International Conference on Robotics and Biomimetics (ROBIO), IEEE, pp. 2267–2272.
- [5] De Luca, A., Oriolo, G., and Samson, C., 1998. “Feedback control of a nonholonomic car-like robot”. In *Robot Motion Planning and Control*. Springer-Verlag, pp. 171–253.
- [6] Poultney, A., Kennedy, C., Clayton, G., and Ashrafiuon, H., 2018. “Robust Tracking Control of Quadrotors Based on Differential Flatness: Simulations and Experiments”. *IEEE/ASME Transactions on Mechatronics*, **23**(3), 6, pp. 1126–1137.
- [7] Cowling, I. D., Yakimenko, O. A., Whidborne, J. F., and Cooke, A. K., 2007. “A prototype of an autonomous controller for a quadrotor UAV”. In 2007 European Control Conference (ECC), IEEE, pp. 4001–4008.
- [8] Agrawal, S., and Sangwan, V., 2008. “Differentially Flat Designs of Underactuated Open-Chain Planar Robots”. *IEEE Transactions on Robotics*, **24**(6), 12, pp. 1445–1451.
- [9] Ren, H., Kumar, A., Wang, X., and Ben-Tzvi, P., 2018. “Parallel Deep Learning Ensembles for Human Pose Estimation”. In Dynamic Systems and Control Conference, ASME, p. V001T07A005.
- [10] Young, T., Hazarika, D., Poria, S., and Cambria, E., 2018. “Recent Trends in Deep Learning Based Natural Language Processing [Review Article]”. *IEEE Computational Intelligence Magazine*, **13**(3), 8, pp. 55–75.
- [11] Riedmiller, M., Hafner, R., Lampe, T., Neunert, M., Degrave, J., Van de Wiele, T., Mnih, V., Heess, N., and Springenberg, J. T., 2018. “Learning by Playing - Solving Sparse Reward Tasks from Scratch”. In Proceedings of Machine Learning Research, pp. 4344–4353.
- [12] Toshani, H., and Farrokhi, M., 2014. “Real-time inverse kinematics of redundant manipulators using neural networks and quadratic programming: A Lyapunov-based approach”. *Robotics and Autonomous Systems*, **62**(6), 6, pp. 766–781.
- [13] Pane, Y. P., Nagesh Rao, S. P., Kober, J., and Babuška, R., 2019. “Reinforcement learning based compensation methods for robot manipulators”. *Engineering Applications of Artificial Intelligence*, **78**, 2, pp. 236–247.
- [14] Ratliff, N., Meier, F., Kappler, D., and Schaal, S., 2016. “DOOMED: Direct Online Optimization of Modeling Errors in Dynamics”. *Big Data*, **4**(4), 12, pp. 253–268.
- [15] Thuruthel, T. G., Falotico, E., Renda, F., and Laschi, C., 2019. “Model-Based Reinforcement Learning for Closed-Loop Dynamic Control of Soft Robotic Manipulators”. *IEEE Transactions on Robotics*, **35**(1), 2, pp. 124–134.
- [16] Watkins, C. J. C. H., 1989. “Learning from Delayed Rewards”. PhD thesis, King’s College.
- [17] Reitermanová, Z. “Data Splitting”. In WDSs 10 Proceedings of Contributed Papers, pp. 31–36.
- [18] Chollet, F., et al., 2015. Keras.
- [19] Abadi, M., Agarwal, A., Barham, P., Brevdo, E., Chen, Z., Citro, C., Corrado, G. S., Davis, A., Dean, J., Devin, M., Ghemawat, S., Goodfellow, I., Harp, A., Irving, G., Isard, M., Jozefowicz, R., Jia, Y., Kaiser, L., Kudlur, M., Levenberg, J., Mané, D., Schuster, M., Monga, R., Moore, S., Murray, D., Olah, C., Shlens, J., Steiner, B., Sutskever, I., Talwar, K., Tucker, P., Vanhoucke, V., Vasudevan, V., Viégas, F., Vinyals, O., Warden, P., Wattemberg, M., Wicke, M., Yu, Y., and Zheng, X., 2015. TensorFlow: Large-Scale Machine Learning on Heterogeneous Systems.
- [20] Bergstra, J., Yamins, D., and Cox, D. D., 2013. Making a Science of Model Search: Hyperparameter Optimization in Hundreds of Dimensions for Vision Architectures. Tech. rep.
- [21] Maas, A. L., Hannun, A. Y., and Ng, A. Y., 2013. “Rectifier Nonlinearities Improve Neural Network Acoustic Models”. In 30th International Conference on Machine Learning.
- [22] MathWorks. Simulink - Simulation and Model-Based Design - MATLAB.